ACS Sustainable Chemistry & Engineering

Research Article

pubs.acs.org/journal/ascecg

Lightweight and Highly Conductive Aerogel-like Carbon from Sugarcane with Superior Mechanical and EMI Shielding Properties

Yuan-Qing Li,*[,†] Yarjan Abdul Samad,[‡] Kyriaki Polychronopoulou,[‡] and Kin Liao*[,†,‡]

[†]Department of Aerospace Engineering, Khalifa University of Science, Technology, & Research, Abu Dhabi 127788, United Arab Emirates

[‡]Department of Mechanical Engineering, Khalifa University of Science, Technology, & Research, Abu Dhabi 127788, United Arab Emirates

Supporting Information

ABSTRACT: Aerogel-like carbon (ALC) based on sugarcane was prepared by a hydrothermal carbonization (HTC) and postpyrolysis process. The ALC prepared from sugarcane exhibits a typical cellular structure with low density, high specific surface area, and excellent electrical conductivity. Although with low density, the specific elastic modulus of ALC can reach 484.7 MPa·cm^3/g, based on our knowledge, this is the strongest aerogel-like carbon ever reported. The average electromagnetic interference (EMI) shielding effectiveness of ALC in X band is 51.0 dB with an absorption-dominant shielding feature. More importantly, the specific surface area of ALC, which has subtle influence on the properties of ALC, can be fined tuned by the HTC process. Considering the chemical-free fabrication process with sustainable raw materials, adjustable structure, excellent mechanical properties, the lightweight and highly conductive ALCs are postulated to have promising potential applications in sensor, energy conversion and storage, and EMI shielding.

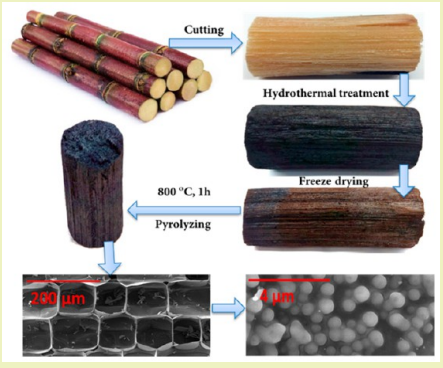

KEYWORDS: *Aerogel-like carbon, Biomass, Hydrothermal, Mechanical, EMI shielding*

INTRODUCTION

Aerogels are a class of materials with porous structure derived from gels, in which the liquid component of the gels has been replaced by air.[1,2] Since the first reports on silica aerogels in 1931, aerogels have been prepared from many materials, such as zeolites, metal oxides, or metal−organic framework.[3] In 1989, the first organic aerogel was reported by Pekala et al., which was formed by the condensation of resorcinol−formaldehyde (RF) in the presence of acid or base catalysts.[3] When compared to other classes of porous materials, organic aerogels are rather competitive in terms of physical properties and performance. This is because, besides being highly porous and lightweight, electrical conductivity could be introduced to organic aerogels by converting them into carbon aerogels. Recently, great potentials of carbon aerogels in various applications, such as sensor, tissue engineering, water treatment, energy conversion and storage, electromagnetic interference (EMI) shielding have been demonstrated.[4−9]

Conventionally, to fabricate carbon aerogel, RF aerogel was pyrolyzed in an inert atmosphere to form a highly cross-linked carbon structure. However, the carbon aerogels prepared always have a high density (100−800 mg·cm^{-3}).[4] To overcome this limitation, aerogel-like carbon (ALC) based on carbon nanotubes (CNT) and graphene has been fabricated in recent years by different methods, including chemical vapor deposition, template, hydrothermal treatment, and freeze-drying.[4,8,9] But harmful and expensive precursors, or complex equipment involved in these syntheses drastically hamper their large-scale production for industry applications.[4]

Given their low cost, sustainable and renewable source, and nontoxicity, biomass has received increasing attention in recent years.[10,11] More importantly, biomass can be directly transformed into carbon materials by a hydrothermal carbonization (HTC) process under mild heating conditions.[12−15] HTC is essentially accelerated coalification of natural biomass down to the time scale of hours and days rather than millions of years.[1] Recently, ALC prepared from water melon, winter melon, and pumpkin by HTC and a postpyrolysis process have been reported by our group, which show great potential in energy conversion and storage, as well as water treatment.[16,17] Unfortunately, although the ALC obtained have low density and high porosity, their specific surface area is quite low (generally less than 10 m^2 g^{-1}). In addition, the mechanical property of those ALCs is poor, which tend to break under compression. Thus, massive production of high performance ALC from biomass is still a great challenge.

Sugarcane is the world's largest crop by production quantity, which accounts approximately 80% of the sugar produced in the world.[18,19] The sugarcane stalks have micrometer-sized lingo-cellulosic vessels and fibrous structures, 12−16 wt % soluble sugars, and 63−73 wt % water, which make them

Received: February 27, 2015
Published: May 13, 2015

DOI: 10.1021/acssuschemeng.5b00340
ACS Sustainable Chem. Eng. 2015, 3, 1419−1427

promising raw materials to fabricate ALC.[20] Here, we report the preparation of ALCs from sugarcane by a HTC and high temperature pyrolysis process, and results from characterizing their structure, electrical conductivies, mechanical behavior, and electromagnetic interference (EMI) shielding performance.

RESULTS AND DISCUSSION

Sugarcane stalks consist of two distinctive parts: (1) nodes and (2) internodes. The cross section of the internode is composed of a rind (outer layer) and pith (inner part). As shown in Figure 1, the sugarcane pith is obtained by removing the rinds and

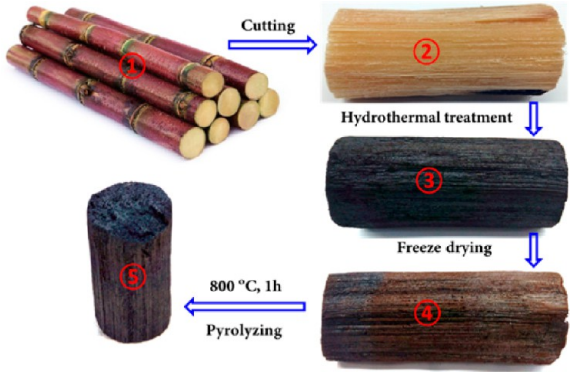

Figure 1. Schematics of ALC preparation: (1) sugarcane stalks, (2) sugarcane pith, (3) carbonaceous sugarcane, (4) aerogel-like sugarcane, (5) aerogel-like carbon.

nodes of sugarcane stalk. After HTC treatment, the sugarcane pith had maintained their original volume and shape, but its color turned from light yellow to black, due to carbonization of sugar inside the pith. Then the dry aerogel-like sugarcane (ALS) was prepared by removing the water within via freeze-drying. The ALS prepared shows a dark brown color, indicating HTC treatment cannot fully convert sugarcane to pure carbon. In addition, the color of ALS obtained via longer HTC time is darker than those via shorter HTC time, indicating a high sugar carbonization rate with long HTC time.

It is well-known that biomass can be converted into carbon via high temperature pyrolysis in an inert atmosphere. Thus, high temperature pyrolysis method was further employed to convert ALS into ALC. To determine the optimal pyrolysis condition, the thermal degradation process of ALS was investigated. As indicated by the thermogravimetric (TG) curve (Figure 2), the main mass loss of ALS, around 73.5%, occurs in the range of 300−400 °C, due to the evaporation of volatile organic species. Furthermore, a high exothermic peak is seen in the differential scanning calorimetric (DSC) curve between 400 and 700 °C, which is associated with the conversion of the organic species to carbon. As revealed by the TG curve, above 700 °C the mass of the sample is graduately stabilized, indicating the formation of aerogel-like carbon. Thus, ALS was pyrolyzed at 800 °C for 1 h to prepare ALC in this work. After pyrolysis, the volume of ALC is only around 50% that of ALS due to the decomposition of the ALS and the evaporation of volatile organic species. The density of sample ALC-1 measured is 0.041 g/cm^3, which is close to that of aerogel-like carbons prepared from other biomass.[16,17] In addition, the element composition of ALC was analyzed by energy-dispersive X-ray spectroscopy (EDS). As revealed in Figure S1 of the Supporting Information, more than 97 at. % of

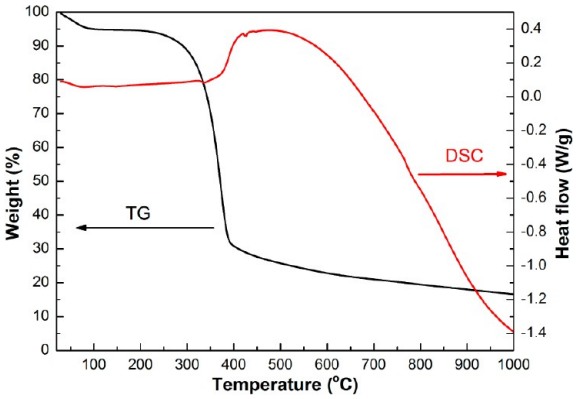

Figure 2. Thermal analysis of aerogel-like sugarcane: TG and DSC curves.

ALC is carbon. At the same time, O and K elements, less than 3 at. % in total, are seen, which is expected for carbon from plants.

Typical macrostructures of ALC from sugarcane in longitudinal and transversal sections are shown in Figure 3. The ALCs prepared have a well-organized cellular structure in the scale of hundreds of micron, which originates from the lingocellulosic cell structure of sugarcane. As shown in Figure 3A,B, along the longitudinal direction (indicated by the red arrow), the sugarcane cell shows a regular rectangular shape, and the cell size varies from several tens of micrometers to more than 100 μm. Compared with longitudinal section, as indicated by Figure 3C,D, the transverse section is less ordered with low uniformity, indicating the anisotoripic nature of the ALC structure. Moreover, it is clear that most of the cells within ALC are closed, indicating low air flow inside ALC. The lowest thermal conductivity of ALC measured is only 0.057 W/(m·K), which is close to the thermal conductivities of general thermal insulation materials such as glass wool (0.045 W/(m·K)), stone wool (0.045 W/(m·K)), and expanded polystyrene (0.041 W/(m·K)).[21]

It is well-known that hydrothermal treatment of saccharides (glucose, sucrose, or starch) can be employed to produce carbonaceous microspheres or nanospheres.[22] Here, the effect of HTC time on structure of ALC was investigated. Scanning electron microscopy (SEM) results show that HTC treatment can only change the micro structure of ALC in the scale of several micrometers, which has no effect on the macrocellular structure of ALC. As revealed in Figure 4A, the surface of ALC-1 in the scale of micrometers is quite smooth, and no particle formation is seen, indicating that 1 h of HTC treatment is not enough for the sugar inside sugarcane cell to carbonize. By prolonging the HTC time, spherical particles start to appear and grow in size. Uniformly distributed spherical particles with an average diameter of 140 nm are clearly seen on the cell wall of ALC-3 (Figure 4B). At the same time, spherical particles are seen at the cell surface of ALS-3 (Figure S2 of the Supporting Information), which confirmed that those particles are formed during HTC treatment. Further prolonging the HTC time to 12 h, as indicated by Figure 4C, the average particle size of ALC-12 has grown to 700 nm. For ALC-48, the average particle size is similar to that of ALC-12, the main difference is that the most of the cell surface of ALC-48 is homogeneously covered by spherical particles. The densities of samples ALC-1, ALC-3, ALC-12, and ALC-48 measured are 0.041, 0.054, 0.112, and 0.121 g/cm^3, respectively, which also confirms that prolonging

DOI: 10.1021/acssuschemeng.5b00340
ACS Sustainable Chem. Eng. 2015, 3, 1419−1427

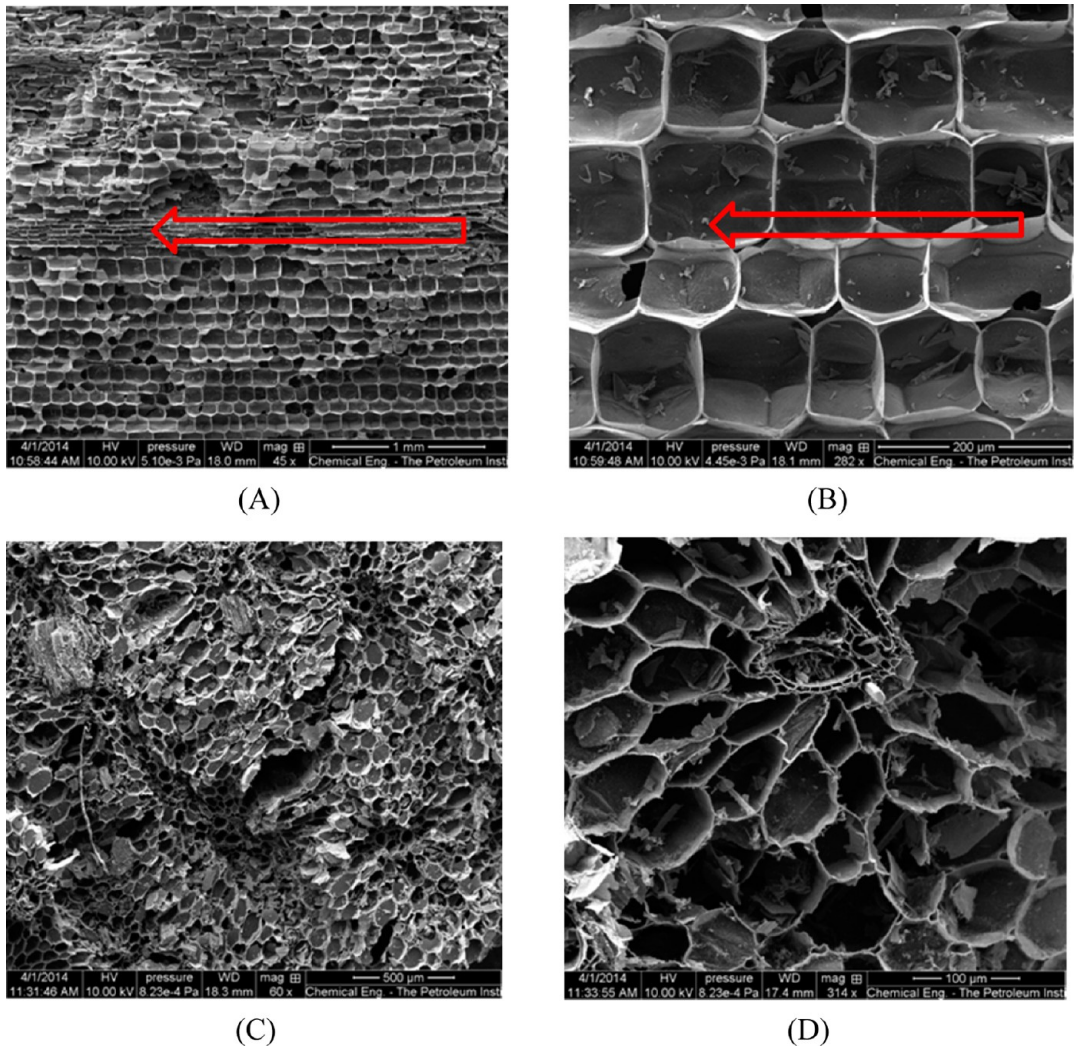

Figure 3. SEM images of aerogel-like carbon from sugarcane: (A and B) longitudinal section of ALC-1, the red arrows indicate the longitudinal direction of sample ALC-1; (C and D) transverse section of ALC-1.

the HTC time can improve the sugar−carbon conversion rate. At the same time, the density of ALC-48 is close to that of ALC-12, indicating that most of the sugar inside the sample has been converted into carbon after 48 h of HTC treatment.

From these results, it is clear that the ALC prepared has a hierarchical structure. The formation process of this structure is depicted schematically in Figure 5. As indicated by Figure 3, the macroscopic structure of ALC, in the scale of hundreds micron, is dominated by the lingocellulosic cell structure of sugarcane and unaffected by HTC treatment. The structure of ALC in micron level is controlled by HTC treatment. After HTC treatment, as revealed in Figures 4 and 5, sugar inside the cell is partially converted to carbon-rich particles with diameter around several hundred nanometers, attaching on the cell surface. By prolonging HTC time, most of sugar content inside the cell is consumed to form more and bigger particles. After pyrolyzing, the whole structure is converted to carbon. Furthermore, different with the loose porous carbon structure formed by merely HTC treatment of sugar, the ALC from sugarcane has a well-connected three-dimensional structure, which offer superior mechanical properties and high electrical conductivity.

N_2 adsorption−desorption isotherms for ALC prepared with different HTC time are shown in Figure 6. The amount of N_2 adsorbed by ALC-1 is very low and close to zero in the whole pressure range. This result agrees well with the SEM observation: the porosity of ALC-1 is in the scale of tens micrometers. After prolonging the HTC time, according to the IUPAC classification, the N_2 adsorption isotherm curves of ALC-3, ALC-12, and ALC-48 exhibited are of type II. At relatively low pressures, the N_2 adsorption quantity increases quickly with the pressure, indicating the existence of a large quantity of micropores. A hysteresis loop at relatively high pressures ($P/P_0 > 0.2$) emerges because of the existence of mesopores and macropores.[23] In addition, based on the adsorption isotherms and the BET formula, the specific surface areas of ALC samples were calculated. The specific surface areas for ALC-1, ALC-3, ALC-12, and ALC-48 are 0, 361, 390, 233 m^2/g, respectively; where ALC-12 has the highest specific surface area.

As revealed by the SEM results and density measurements, the sugar−carbon nanoparticles conversion rate of ALC-12 is higher than those of ALC-3 and ALC-1, which leads to its high specific surface area. Although the sugar−carbon conversion rate of ALC-48 is even higher than that of ALC-12, all the carbon nanoparticles formed in ALC-48 stacked more compactly than ALC-12, resulting in lower specific surface area. Actually, by directly freeze-drying sugarcane and

DOI: 10.1021/acssuschemeng.5b00340
ACS Sustainable Chem. Eng. 2015, 3, 1419−1427

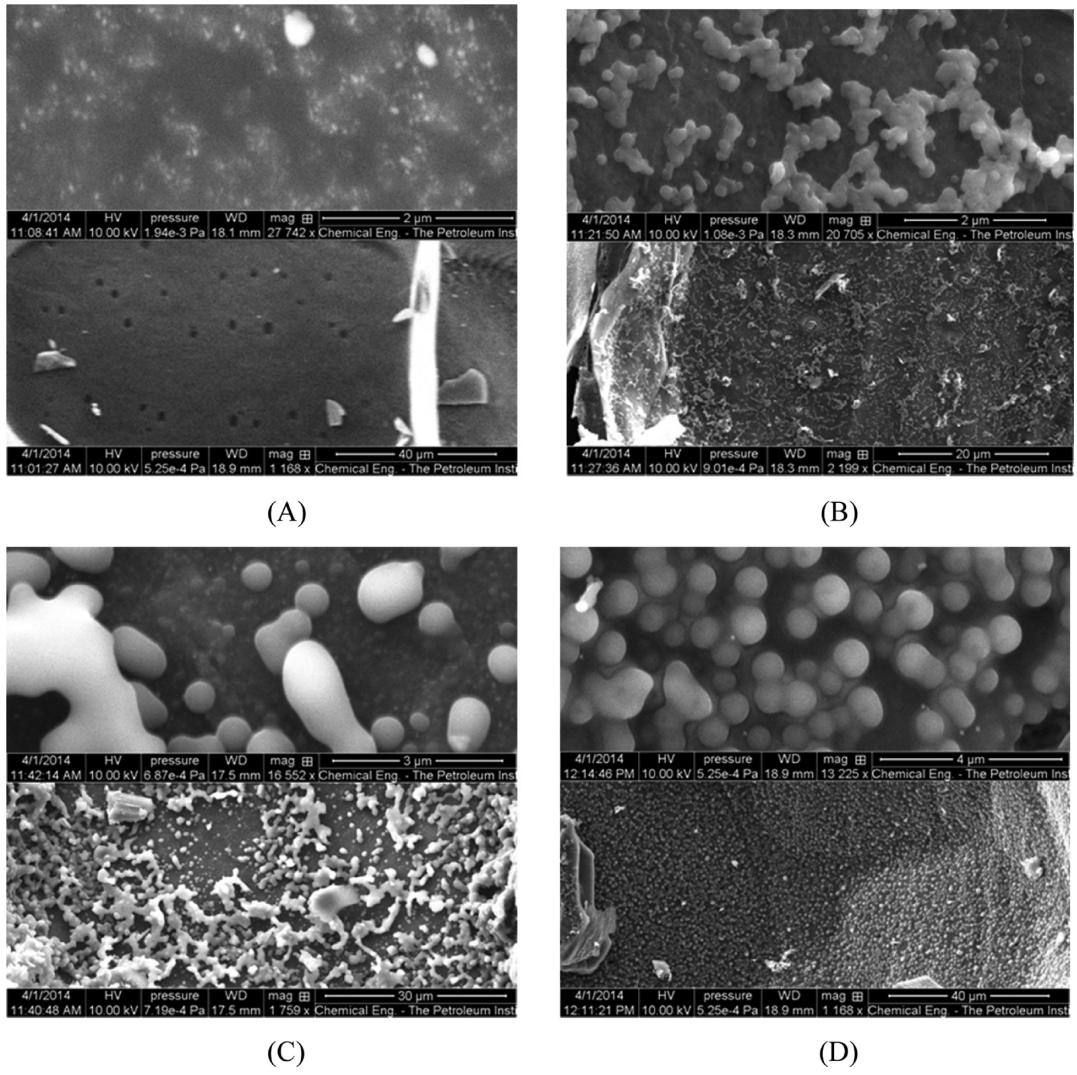

Figure 4. Effect of HTC time on the structure of ALC: the SEM images of (A) ALC-1, (B) ALC-3, (C) ALC-12, and (D) ALC-48, showing the process of carbon nanoparticles growth.

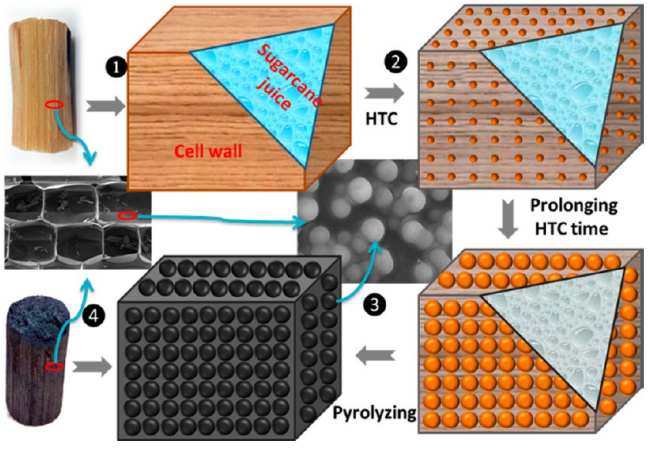

Figure 5. Schematics of formation of ALC with hierarchical structure: (1) single cell of sugarcane with sugar rich juice inside; (2) after HTC treatment, sugar is partially converted to carbon-rich particles, attach themselves on the cell surface; (3) by prolonging HTC time, most of sugar inside the cell is consumed to form more and bigger particles; (4) after pyrolyzing, the whole structure is converted to carbon.

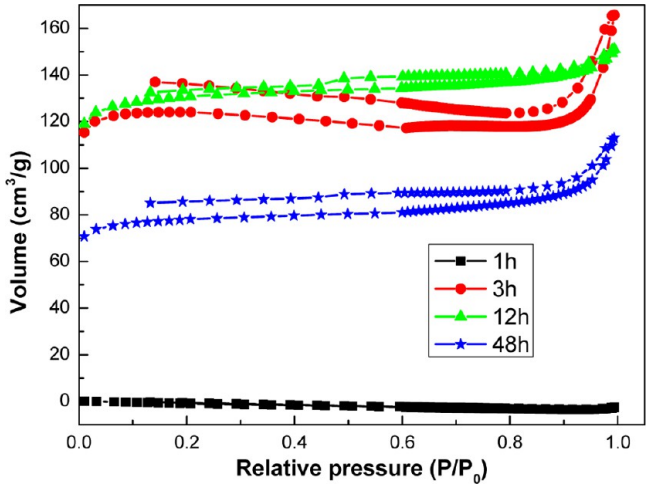

Figure 6. N_2 adsorption−desorption isotherms of ALC prepared with different HTC times.

conducting postpyrolysis, ALC can be prepared without pre-HTC treatment (ALC-N-HTC). Although the density of ALC-N-HTC is close to that of ALC-48, the structure of ALC-N-

DOI: 10.1021/acssuschemeng.5b00340
ACS Sustainable Chem. Eng. 2015, 3, 1419−1427

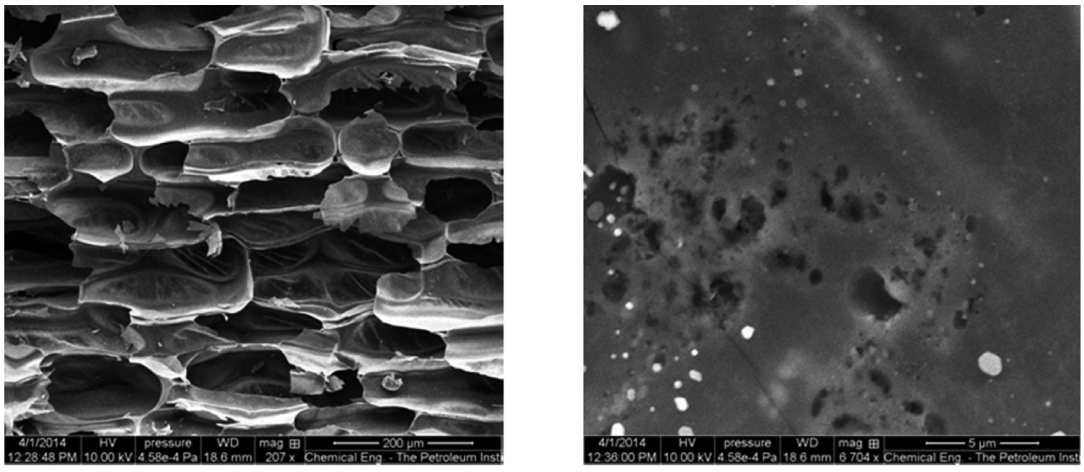

Figure 7. SEM images of ALC-N-HTC with low (A) and high (B) magnification.

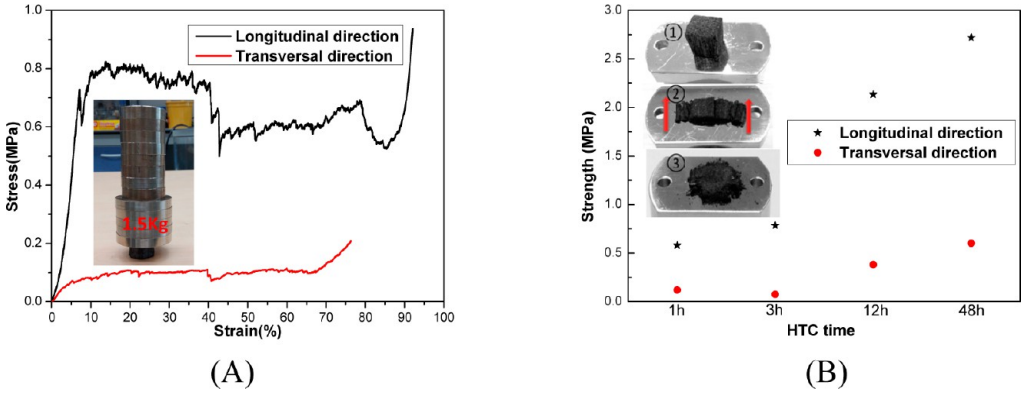

Figure 8. (A) Typical compressive stress−strain curves of ALC along the longitudinal and transversal direction; inset: ALC loaded with 1.5 kg steel weight. (B) Effect of HTC time on the compressive strength of SCA along the longitudinal and transversal direction; inset: ALC samples before compression ①, failed sample in the transversal direction ②, and failed sample in the longitudinal direction ③.

Table 1. Properties of ALC Prepared with Different HTC Times

properties	ALC-1	ALC-3	ALC-12	ALC-48
density (g/cm^3)	0.041	0.0539	0.112	0.121
electrical conductivity (S/m)	41.5	61.9	96.4	133.3
thermal conductivity (W/(m·K))	0.0567	0.0641	0.0828	0.0992
specific surface area (m^2/g)	0	361	390	233
compression strength - transversal direction (MPa)	0.119	0.075	0.380	0.6013
compression strength - longitudinal direction (MPa)	0.580	0.785	2.134	2.719
elastic modulus - transversal direction (MPa)	1.49	1.24	13.38	19.98
elastic modulus - longitudinal direction (MPa)	21.19	20.61	51.55	58.65
average EMI SE in X band	28.12	42.73	50.99	44.64

HTC is similar to ALC-1 (Figure 7). The cell surface of ALC-N-HTC at the micrometer scale is quite smooth, and areas covered by carbon nanoparticles are not seen (Figure 7B). At the same time, the specific surface area measured is close to zero. These results reveal that HTC treatment is critical to obtain ALC with hierarchical structure and high specific surface area.

The ALCs prepared exhibit excellent mechanical properties, as shown in the inset of Figure 8A, where a piece of ALC with diameter around 2 cm could support a 1.5 kg load, equivalent to 5000 times its own weight. Quasi-static compression tests were performed to evaluate the mechanical performance of ALC using a microforce tester. Typical stress−strain curves of the ALC along the longitudinal and transversal direction are displayed in Figure 8A. Under compression, ALC samples tested exhibit three stages of elastic−brittle deformation, in accord with the typical compression deformation of cellular carbon foams.[24] It is clear that the ALC exhibit a linear elastic behavior at low strain, typically less than 10%, attributing to the elastic distorting of the cell edges and walls. Further loading results in a nonlinear deformation, a long serrated plateau is seen after the elastic threshold, typically from around 10% up to 80% strain. The peak value denotes the point of crack initiation. Layered crushing mode of failure occurs in the ALC: during

DOI: 10.1021/acssuschemeng.5b00340
ACS Sustainable Chem. Eng. 2015, 3, 1419−1427

Table 2. Comparison of Specific Modulus between ALC-48 and Aerogel-like Materials from the Literature[9,25−34]

type of aerogel	modulus (MPa)	density (g/cm^3)	specific modulus (MPa·cm^3/g)	reference
ceramic fiber-reinforced carbon aerogel	6.83	0.29	23.6	25
flexible superhydrophobic silica aerogels	0.083	0.05	1.66	26
aerogels based on nanofibrillated cellulose	2.8	0.105	26.7	27
methylsilsesquioxane aerogels	7.41	0.22	33.68	28
resorcinol-formaldehyde aerogel	33	0.24	137.5	29
polymer−silica aerogel composites	4.29	0.23	18.65	30
graphene oxide aerogels	22	0.06	367	31
graphene-based cellular monoliths	0.033	0.0066	5	32
graphene coated carbon nanotube aerogels	0.75	0.014	53.6	33
graphene−CNT composite aerogel	0.329	0.0056	58.8	9
carbon nanotube sponge with carbon coating	4.86	0.05	97.2	34
ALC-48 along longitudinal direction	58.65	0.121	484.7	this report
ALC-48 along transversal direction	19.98	0.121	165.1	this report

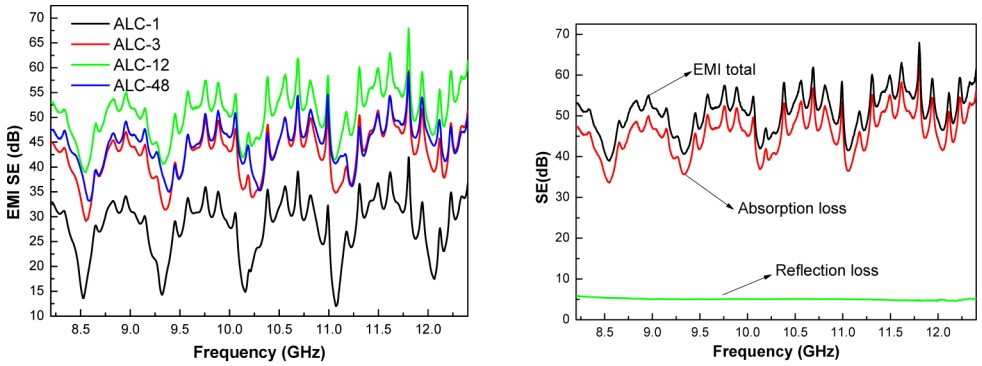

Figure 9. (A) EMI shielding effectiveness of ALCs in the X-band frequency range, (B) comparison of SE_{total}, SE_A, and SE_R of ALC-12 in X band.

compression, each time one layer of cells collapse in a brittle manner, the load is recovered when the next layer of cells is being compressed. After most of the cells have collapsed, a densification regime appears. Moreover, as indicated by Figure 8A, the compression stress of ALC along longitudinal direction (growth direction) is at least 4 times higher than that in transverse direction. The insets of Figure 8B are the appearance of ALC samples before and after compression. After compression along the transverse direction, the sample has collapsed to rod-like bundles. In contrast, a pile of powder is seen for samples failed along longitudinal direction. Obviously, to crush the sample along longitudinal direction consumes more energy than that along transverse direction. As confirmed by SEM results, this mechanical anisotropy originates from the anisotropic structure of ALC.

The effect of HTC time on the mechanical properties of ALC was investigated. On the basis of the stress−strain curves obtained, compressive yield strength and elastic modulus along longitudinal and transversal direction were calculated and presented in Figure 8B and Table 1. As expected, increasing the HTC time has a significant effect on the mechanical properties of ALC. The yield strength and elastic modulus of the ALC both gradually increase with an increase of the HTC time. The average yield strengths along longitudinal direction of ALC-1, ALC-3, ALC-12, and ALC-48 are 0.58, 0.78, 2.13, and 2.72 MPa, respectively, showing an obvious increasing trend. This increase may attribute to improved sugar−carbon conversion efficiency after longer HTC treatment, which leads to the formation of a thicker cell wall with higher strength.

Furthermore, the mechanical properties of ALC-N-HTC were also investigated. As indicated by Figure S3 of the Supporting Information, the compression behavior of ALC-N-HTC is similar to that of ALC. The compression strengths of ALC-N-HTC along transversal and longitudinal direction are 0.31 and 0.70 MPa, respectively, which are better than ALC-1's, but weaker than ALC-48's. To compare over a broader spectrum of materials, the specific modulus of ALC-48 and other aerogel-like materials from literature were calculated and listed in Table 2. It is seen that ALC-48 out-performances many native aerogels, including fiber-reinforced carbon aerogels.[25−30] They are also stronger than graphene aerogel or CNT aerogel reported previously.[9,31−34] On the basis of our knowledge, ALC-48 prepared is the strongest aerogel-like carbon ever reported. These excellent mechanical properties of ALC attribute to the special cell structure of sugarcane stalks. These excellent mechanical properties are essential for various applications, such as energy absorption lightweight structural components.

The ultralight and high porosity ALC prepared is also electrical conductive: when connected in a circuit, an LED lamp is illumined (Figure S4 of the Supporting Information). The electrical conductivities of ALC-1, ALC-3, ALC-12, and ALC-48 are 41.5, 61.9, 96.4, and 133.3 S/m, respectively, showing an obvious increasing trend with increasing HTC time. The excellent electrical conductivity is attributed to the interconnected three-dimensional network formed by the sugarcane cells, which provides a fast electron transport channel.

DOI: 10.1021/acssuschemeng.5b00340
ACS Sustainable Chem. Eng. 2015, 3, 1419−1427

In recent years, the rapid development of electronic systems and telecommunications has led to serious concerns regarding electromagnetic pollution. Electromagnetic interference (EMI) shielding materials are needed to protect the workspace and environment from such radiation.[35−37] It is well-known that high electrical conductivity and lightweight are two important technical requirements for effective and practical EMI shielding applications, which make ALC a potential option as an EMI shielding material.

The EMI shielding effectiveness (SE) of a material is defined as SE (dB) = $-10 \log(P_t/P_0)$, where P_t and P_0 are transmitted and incident electromagnetic power, respectively. For example, a material with 20 dB EMI shielding effectiveness (needed for commercial applications) leaves only 1% of electromagnetic waves to be transmitted. Figure 9A shows the EMI shielding effectiveness of SCA samples (10 mm thick) over the frequency range of 8.2−12.4 GHz (X band). It is obvious that all the ALCs prepared show high EMI shielding effectiveness with wave-like curves in X band. Identical patterns were reported for graphene and CNT nanocomposites, and such behavior is attributed to the irregular nature of the conductive networks.[35,38] The average EMI SE values in X band for ALC-1, ALC-3, ALC-12, and ALC-48 are 28.1, 42.7, 51.0, and 44.6 dB, respectively. Because of low density and electrical conductivity, it is expected that the EMI SE values of ALC-1 and ALC-3 are lower than that of ALC-12. However, although ALC-48 has the highest density and conductivity, the EMI SE of ALC-48 is lower than that of ALC-12. Obviously, the MEI SE is not only related with the electrical conductivity but also related to the material structure.

When an electromagnetic wave is incident on a shielding material, the incident power is divided into reflected power, absorbed power, and transmitted power. EMI is attenuated by reflection (include multireflection) and/or absorption, and the total EMI shielding effectiveness (SE_{total}) is the sum of absorption loss (SE_A) and reflection loss (SE_R). Figure 9B shows the representative of SE_{total}, SE_A, and SE_R of SCA in the X-band frequency. It is clear that the contribution of absorption to the EMI shielding is much higher than that of reflection. For instance, the absorption loss and reflection loss of ALC-12 contribute to 90% and 10% of the total EMI SE, respectively. As indicated in Figure S5 of the Supporting Information, regardless of HTC time, all ALCs prepared are both reflective and absorptive to electromagnetic radiation in the X-band frequency, and absorption is the dominant shielding mechanism.

In addition to the reflection and absorption mechanisms, multiple-reflection loss is also an important shielding mechanism for the porous materials. When the electromagnetic wave is incident on the cellular structure of an ALC, it is difficult for the wave to escape from the material until it is mostly absorbed. Because the specific surface area of ALC-12 is much higher than that of ALC-48, which causes more reflection inside the pores and resulted in the highest EMI SE_{total} and EMI SE_A.

Compared with other aerogel-like materials, the ALC from sugarcane shows remarkable advantages: (i) the raw material to prepare SCA is low-cost and sustainable, and the fabrication process is simple and chemical-free; (ii) the unique cellular structure of ALC simultaneously offers superior mechanical properties and high electrical conductivity; (iii) the specific surface area of ALC, which has subtle influence on the properties of ALC, can be fined tuned by the HTC process because of the high sugar content of surgarcane stalks. Furthermore, the EMI shielding effectiveness of ALC in X band can reach 51.0 dB with an absorption-dominant shielding feature, indicating that ALC can be an excellent candidate as effective and lightweight EMI shielding materials.

CONCLUSION

In conclusion, ALCs have been prepared by HTC of sugarcane stalks and a postpyrolysis process. The ALCs prepared exhibit a well-organized cellular structure with low density, low thermal conductivity, high specific surface area, and high electrical conductivity. The compression strength and specific elastic modulus of ALC can reach 2.72 and 484.7 MPa·cm^3/g, respectively; on the basis of our knowledge, this is the strongest aerogel-like carbon ever reported. After HTC treatment, uniformly distributed spherical carbon nanoparticles were formed on the cell wall of ALC, which has great effect on the overall properties of ALC prepared. In addition, the highest EMI SE of ALC in X band is 51.0 dB with an absorption-dominant shielding feature. More importantly, the fabrication process of ALC is chemical-free with biomass−sugarcane as raw materials, and the structures and properties of ALC can be fine-tuned by controlling HTC time. ALCs are postulated to have promising applications in sensors, energy conversion and storage, EMI shielding, and more.

EXPERIMENTAL METHODS

Preparation of ALC. First, the rinds and joint parts of sugarcane stalks obtained from local market were carefully removed by knife. The pith of a sugarcane stalk was cut into appropriate dimensions, and placed into a Teflon-lined stainless steel autoclave. Carbonaceous sugarcane monoliths were obtained by heating the autoclaves with sugarcane under self-generated pressure at 180 °C for 1, 3, 12, and 48 h, respectively. The carbonaceous sugarcane monoliths were immersed in hot water around 80 °C for 10 h to remove the soluble impurities. Then, the aerogel-like sugarcanes (ALSs) were obtained by freeze-drying the carbonaceous sugarcane monoliths obtained. Finally, to convert fully the ALS to aerogel-like carbon, the ALSs obtained were placed in a tube furnace and pyrolyzed at 800 °C for 1 h in N_2 atmosphere. The aerogel-like carbons prepared via different HTC times were named as ALC-1, ALC-3, ALC-12, and ALC-48, respectively, where the suffix indicates time of HTC treatment in hours.

Characterization. All optical pictures used in this paper were taken by a Canon digital camera (IXUS 70). The thermal degradation process of aerogel-like sugarcane was investigated by a simultaneous thermogravimetry and differential scanning calorimetry (TG-DSC, TA SDT 600) analysis. The morphologies of ALC were imaged by a scanning electron microscopy (SEM, FEI Quanta FEG 250) instrument under a voltage of 10 kV, samples for SEM were carefully broke from ALC along different directions. Porosimetry measurements were carried out using a high-resolution 3Flex Micromeritics adsorption instrument equipped with high-vacuum system and three 0.1 Torr pressure transducers. Densities were calculated by measuring the weight and volume of the ALC samples. The electrical conductivities of ALC were measured using a four-point probe resistivity measurement system (RST 8, 4 Probs Tech). For all the density and electrical conductivity measurements, more than 8 samples were tested.

The compressive behavior of ALC was investigated using a Micro Tester (Instron 5948) at a loading rate of 1 mm/min, the dimension of tested samples is around 8 mm × 8 mm × 8 mm. The compression yield strength is obtained from the end of the initial linear region of stress−strain curve. The compressive elastic modulus is calculated from the initial linear region of the stress−strain curves. The thermal conductivities of ALC from sugarcane were measured using a TPS

DOI: 10.1021/acssuschemeng.5b00340
ACS Sustainable Chem. Eng. 2015, 3, 1419−1427

2500S thermal property system equipped with 3.2 mm radius sensor. The samples used for thermal conductivity measurement were cut to a cylinder shape, and the thickness and radius of samples are around 20 and 10 mm, respectively.

For the EMI shielding effectiveness (SE) characterization in the X-band (8.2−12.4 GHz) frequency, a network analyzer (Agilent, E5071C ENA) connected with a rectangular waveguide (WR-90) was used. Rectangular specimens with the thickness of 10 mm were placed between the two sections of the waveguide, and the S-parameters (S_{11}, S_{12}, S_{22}, S_{21}) of each sample were recorded over the X-band frequency. The overall EMI SE was calculated based on the *S*-parameters as follows[38]

$$\text{EMI SE} = 10\log\frac{1}{|S_{12}|^2} = 10\log\frac{1}{|S_{21}|^2} \quad (1)$$

where $|S_{ij}|^2$ represents the power transmitted from port i to port j. Total shielding (SE_T), absorption loss (SE_A), reflection loss (SE_R) were calculated based on the *S*-parameters obtained from the vector network analyzer as follows

$$SE_T = SE_R + SE_A \quad (2)$$

$$SE_R = 10\log_{10}\left(\frac{1}{1-|S_{11}|^2}\right) \quad (3)$$

$$SE_A = 10\log_{10}\left(\frac{1-|S_{11}|^2}{|S_{12}|^2}\right) \quad (4)$$

■ ASSOCIATED CONTENT

Supporting Information

Energy-dispersive X-ray spectroscopy and element composition of ALC, SEM images of ALS-3 with different magnifications, typical compressive stress−strain curves of ALC-N-HTC along the longitudinal and transversal directions, circuit constructed with the ALC as lightweight conductive bulk, and effect of HTC time on the EMI shielding effectiveness of ALC: absorption loss and reflection loss. The Supporting Information is available free of charge on the ACS Publications website at DOI: 10.1021/acssuschemeng.5b00340.

■ AUTHOR INFORMATION

Corresponding Authors

*Y.-Q. Li. E-mail: yuanqing.li@kustar.ac.ae.
*K. Liao. E-mail: kin.liao@kustar.ac.ae.

Notes

The authors declare no competing financial interest.

■ ACKNOWLEDGMENTS

The authors are grateful to the financial support by Khalifa University Internal Research Funds (No. 210038, 210014 and 210047).

■ REFERENCES

(1) Wohlgemuth, S.-A.; Fellinger, T.-P.; Jaeker, P.; Antonietti, M. Tunable nitrogen-doped carbon aerogels as sustainable electrocatalysts in the oxygen reduction reaction. *J. Mater. Chem. A* **2013**, *1* (12), 4002−4009.

(2) Wu, X. L.; Wen, T.; Guo, H. L.; Yang, S. B.; Wang, X. K.; Xu, A. W. Biomass-derived sponge-like carbonaceous hydrogels and aerogels for supercapacitors. *ACS Nano* **2013**, *7* (4), 3589−3597.

(3) Antonietti, M.; Fechler, N.; Fellinger, T.-P. Carbon aerogels and monoliths: Control of porosity and nanoarchitecture via sol-gel routes. *Chem. Mater.* **2014**, *26* (1), 196−210.

(4) Wu, Z. Y.; Li, C.; Liang, H. W.; Chen, J. F.; Yu, S. H. Ultralight, flexible, and fire-resistant carbon nanofiber aerogels from bacterial cellulose. *Angew. Chem., Int. Ed.* **2013**, *52* (10), 2925−2929.

(5) Fellinger, T.-P.; White, R. J.; Titirici, M.-M.; Antonietti, M. Borax-mediated formation of carbon aerogels from glucose. *Adv. Funct. Mater.* **2012**, *22* (15), 3254−3260.

(6) Li, N.; Zhang, Q.; Gao, S.; Song, Q.; Huang, R.; Wang, L.; Liu, L. W.; Dai, J. W.; Tang, M. L.; Cheng, G. S. Three-dimensional graphene foam as a biocompatible and conductive scaffold for neural stem cells. *Sci. Rep* **2013**, *3*, 1604.

(7) Li, Y.; Samad, Y. A.; Liao, K. From cotton to wearable pressure sensor. *J. Mater. Chem. A* **2015**, *3* (5), 2181−2187.

(8) Samad, Y. A.; Li, Y.; Schiffer, A.; Alhassan, S. M.; Liao, K. Graphene foam developed with a novel two-step technique for low and high strains and pressure-sensing applications. *Small* **2015**, DOI: 10.1002/smll.201403532.

(9) Sun, H.; Xu, Z.; Gao, C. Multifunctional, ultra-flyweight, synergistically assembled carbon aerogels. *Adv. Mater.* **2013**, *25* (18), 2554−2560.

(10) Chen, W.-H.; Ye, S.-C.; Sheen, H.-K. Hydrothermal carbonization of sugarcane bagasse via wet torrefaction in association with microwave heating. *Bioresour. Technol.* **2012**, *118*, 195−203.

(11) Bi, H. C.; Yin, Z. Y.; Cao, X. H.; Xie, X.; Tan, C. L.; Huang, X.; Chen, B.; Chen, F. T.; Yang, Q. L.; Bu, X. Y.; Lu, X. H.; Sun, L. T.; Zhang, H. Carbon fiber aerogel made from raw cotton: A novel, efficient and recyclable sorbent for oils and organic solvents. *Adv. Mater.* **2013**, *25* (41), 5916−5921.

(12) Zhao, Y.-C.; Zhao, L.; Mao, L.-J.; Han, B.-H. One-step solvothermal carbonization to microporous carbon materials derived from cyclodextrins. *J. Mater. Chem. A* **2013**, *1* (33), 9456−9461.

(13) Titirici, M. M.; Thomas, A.; Yu, S. H.; Muller, J. O.; Antonietti, M. A direct synthesis of mesoporous carbons with bicontinuous pore morphology from crude plant material by hydrothermal carbonization. *Chem. Mater.* **2007**, *19* (17), 4205−4212.

(14) Hu, B.; Wang, K.; Wu, L. H.; Yu, S. H.; Antonietti, M.; Titirici, M. M. Engineering carbon materials from the hydrothermal carbonization process of biomass. *Adv. Mater.* **2010**, *22* (7), 813−828.

(15) White, R. J.; Budarin, V.; Luque, R.; Clark, J. H.; Macquarrie, D. J. Tuneable porous carbonaceous materials from renewable resources. *Chem. Soc. Rev.* **2009**, *38* (12), 3401−3418.

(16) Li, Y.-Q.; Samad, Y. A.; Polychronopoulou, K.; Alhassan, S. M.; Liao, K. Carbon aerogel from winter melon for highly efficient and recyclable oils and organic solvents absorption. *ACS Sustainable Chem. Eng.* **2014**, *2* (6), 1492−1497.

(17) Li, Y.; Samad, Y. A.; Polychronopoulou, K.; Alhassan, S. M.; Liao, K. From biomass to high performance solar-thermal and electric-thermal energy conversion and storage materials. *J. Mater. Chem. A* **2014**, *2* (21), 7759−7765.

(18) Foo, K. Y.; Lee, L. K.; Hameed, B. H. Preparation of activated carbon from sugarcane bagasse by microwave assisted activation for the remediation of semi-aerobic landfill leachate. *Bioresour. Technol.* **2013**, *134*, 166−172.

(19) Crop production. http://en.wikipedia.org/wiki/Food_and_Agriculture_Organization_of_the_United_Nations.

(20) Chou, T.-c.; Huang, C.-h.; Doong, R.-a. Fabrication of hierarchically ordered porous carbons using sugarcane bagasse as the scaffold for supercapacitor applications. *Synth. Met.* **2014**, *194*, 29−37.

(21) Papadopoulos, A. M. State of the art in thermal insulation materials and aims for future developments. *Energy Build.* **2005**, *37* (1), 77−86.

(22) Romero-Anaya, A. J.; Ouzzine, M.; Lillo-Rodenas, M. A.; Linares-Solano, A. Spherical carbons: Synthesis, characterization and activation processes. *Carbon* **2014**, *68*, 296−307.

(23) Li, M.; Li, W.; Liu, S. Hydrothermal synthesis, characterization, and KOH activation of carbon spheres from glucose. *Carbohydr. Res.* **2011**, *346* (8), 999−1004.

(24) Szczurek, A.; Fierro, V.; Pizzi, A.; Stauber, M.; Celzard, A. Carbon meringues derived from flavonoid tannins. *Carbon* **2013**, *65*, 214−227.

DOI: 10.1021/acssuschemeng.5b00340
ACS Sustainable Chem. Eng. 2015, 3, 1419−1427

(25) Yang, J.; Li, S.; Luo, Y.; Yan, L.; Wang, F. Compressive properties and fracture behavior of ceramic fiber-reinforced carbon aerogel under quasi-static and dynamic loading. *Carbon* **2011**, *49* (5), 1542−1549.
(26) Nadargi, D. Y.; Latthe, S. S.; Hirashima, H.; Rao, A. V. Studies on rheological properties of methyltriethoxysilane (MTES) based flexible superhydrophobic silica aerogels. *Microporous Mesoporous Mater.* **2009**, *117* (3), 617−626.
(27) Sehaqui, H.; Zhou, Q.; Berglund, L. A. High-porosity aerogels of high specific surface area prepared from nanofibrillated cellulose (NFC). *Compos. Sci. Technol.* **2011**, *71* (13), 1593−1599.
(28) Kanamori, K.; Aizawa, M.; Nakanishi, K.; Hanada, T. New transparent methylsilsesquioxane aerogels and xerogels with improved mechanical properties. *Adv. Mater.* **2007**, *19* (12), 1589−+.
(29) Yang, J.; Li, S.; Yan, L.; Liu, J.; Wang, F. Compressive behaviors and morphological changes of resorcinol-formaldehyde aerogel at high strain rates. *Microporous Mesoporous Mater.* **2010**, *133* (1−3), 134−140.
(30) Boday, D. J.; Stover, R. J.; Muriithi, B.; Keller, M. W.; Wertz, J. T.; Obrey, K. A. D.; Loy, D. A. Strong, low-density nanocomposites by chemical vapor deposition and polymerization of cyanoacrylates on aminated silica aerogels. *ACS Appl. Mater. Interfaces* **2009**, *1* (7), 1364−1369.
(31) Huang, H.; Chen, P.; Zhang, X.; Lu, Y.; Zhan, W. Edge-to-edge assembled graphene oxide aerogels with outstanding mechanical performance and superhigh chemical activity. *Small* **2013**, *9* (8), 1397−1404.
(32) Qiu, L.; Liu, J. Z.; Chang, S. L. Y.; Wu, Y.; Li, D. Biomimetic superelastic graphene-based cellular monoliths. *Nat. Commun.* **2012**, *3*.
(33) Kim, K. H.; Oh, Y.; Islam, M. F. Graphene coating makes carbon nanotube aerogels superelastic and resistant to fatigue. *Nat. Nanotechnol.* **2012**, *7* (9), 562−566.
(34) Zhao, W.; Li, Y.; Wang, S.; He, X.; Shang, Y.; Peng, Q.; Wang, C.; Du, S.; Gui, X.; Yang, Y.; Yuan, Q.; Shi, E.; Wu, S.; Xu, W.; Cao, A. Elastic improvement of carbon nanotube sponges by depositing amorphous carbon coating. *Carbon* **2014**, *76*, 19−26.
(35) Chen, Z. P.; Xu, C.; Ma, C. Q.; Ren, W. C.; Cheng, H. M. Lightweight and flexible graphene foam composites for high-performance electromagnetic interference shielding. *Adv. Mater.* **2013**, *25* (9), 1296−1300.
(36) Liang, J. J.; Wang, Y.; Huang, Y.; Ma, Y. F.; Liu, Z. F.; Cai, F. M.; Zhang, C. D.; Gao, H. J.; Chen, Y. S. Electromagnetic interference shielding of graphene/epoxy composites. *Carbon* **2009**, *47* (3), 922−925.
(37) Li, N.; Huang, Y.; Du, F.; He, X. B.; Lin, X.; Gao, H. J.; Ma, Y. F.; Li, F. F.; Chen, Y. S.; Eklund, P. C. Electromagnetic interference (EMI) shielding of single-walled carbon nanotube epoxy composites. *Nano Lett.* **2006**, *6* (6), 1141−1145.
(38) Al-Saleh, M. H.; Saadeh, W. H.; Sundararaj, U. EMI shielding effectiveness of carbon based nanostructured polymeric materials: A comparative study. *Carbon* **2013**, *60*, 146−156.

DOI: 10.1021/acssuschemeng.5b00340
ACS Sustainable Chem. Eng. 2015, 3, 1419−1427